Sensorless Sine-Wave Controller IC for PM Brushless Motor Employing Automatic Lead-Angle Compensation

Minki Kim, Sewan Heo, Jimin Oh, Jung-Hee Suk, Yil Suk Yang, Ki-Tae Park, and Jinsung Kim

This paper presents an advanced sensorless permanent magnet (PM) brushless motor controller integrated circuit (IC) employing an automatic lead-angle compensator. The proposed IC is composed of not only a sensorless sine-wave motor controller but also an isolated gate-driver and current self-sensing circuit. The fabricated IC operates in sensorless mode using a position estimator based on a sliding mode observer and an open-loop start-up. For high efficiency PM brushless motor driving, an automatic lead-angle control algorithm is employed, which improves the efficiency of a PM brushless motor system by tracking the minimum copper loss under various load and speed conditions. The fabricated IC is evaluated experimentally using a commercial 200 W PM brushless motor and power switches. The proposed IC is successfully operated without any additional sensors, and the proposed algorithm maintains the minimum current and maximum system efficiency under 0 N·m to 0.8 N·m load conditions. The proposed IC is a feasible sensorless speed controller for various applications with a wide range of load and speed conditions.

Keywords: Automatic lead-angle compensation, motor control IC, sensorless drive.

Manuscript received Apr. 20, 2015; revised Oct. 1, 2015; accepted Oct. 12, 2015.

This work was supported by the IT R&D program of MKE/KEIT (10035171, Development of High Voltage/Current Power Module and ESD for BLDC Motor).

Minki Kim (corresponding author, mkk@etri.re.kr), Jimin Oh (ojmhiin@etri.re.kr), Jung-Hee Suk (jhsuk@etri.re.kr), and Yil Suk Yang (ysyang@etri.re.kr) are with the Information & Communications Core Technology Research Laboratory, ETRI, Daejeon, Rep. of Korea.

Sewan Heo (sewany@etri.re.kr) is with the IT Convergence Technology Research Laboratory, ETRI, Daejeon, Rep. of Korea.

Ki-Tae Park (kt2000.park@irondevice.com) and Jinsung Kim (npstar@irondevice.com) are with the Iron Device Corporation, Seoul, Rep. of Korea.

I. Introduction

With increasing attention being given to global warming and energy conservation, the energy saving of electrical systems is becoming increasingly required in various types of electronic equipment and systems [1]–[2]. A permanent magnet (PM) brushless motor system has received considerable attention in industries and consumer appliances owing to its high efficiency, high power density, and wide range of suitable applications [1]–[2].

To develop high-performance motor driving systems, motor control algorithms and related devices have been studied for several decades by various research groups [2]–[5]. For future advanced devices, motor controllers need to be optimized for application targets through a simple and cost-effective design. There are several design methods for building a motor controller, such as a high-performance general-purpose processor and FPGA; however, in terms of performance and cost, it is necessary to design the right kind of integrated circuit (IC) [6]. In an effort to design a sensorless motor controller, a number of attempts using various motor control algorithms have been reported [7]–[15]. A square-wave motor driving algorithm is useful for the design of an application-specific integrated circuit (ASIC) technique because it has the advantages of a simple algorithm and easy circuit design for sensorless control [7]–[8]. A vector-based control algorithm is the most popular type of motor control method owing to its high performance, but it is difficult to design for an ASIC owing to its complexity [9]–[11]. The open-loop based V/f control method can be applied without a rotor position signal; however, it is unsuitable for

high efficiency driving under a wide range of load and speed conditions [12]–[13]. The six-step-based sine-wave control method has a simple circuit design and good performance, and controls the motor as a sinusoidal current without a complex d-q axis transformation; however, its sensorless algorithm needs to be improved [14]–[15].

For high efficiency motor driving, the maximum torque per ampere (MTPA) using a current control method has been utilized in high-performance vector control systems. The MTPA method controls the mismatched component in the d-q reference frame analysis of a three-phase current, which can improve the motor driving efficiency [16]–[17]. The lead-angle compensation of the hall sensor signal–based 120/180 degree drive improves the driving efficiency for special load/speed conditions, but it is necessary to improve the accuracy and performance up to the level of the MTPA algorithm [17]–[19].

The purpose of our work is to propose an advanced sensorless sine-wave controller with a simple design and efficient performance. The proposed IC is composed of not only a sensorless sine-wave motor controller but also an isolated gate-driver and current self-sensing circuit. For efficient driving in sensorless mode, the proposed IC is successfully confirmed within a wide range of load operations by suppressing the driving loss. Using the fabricated motor-driving ICs, the automatic lead-angle compensation is evaluated experimentally in a 200 W PM brushless motor system. The automatic lead-angle compensator reduces the amplitude of the three-phase current by controlling the phase difference of the phase current and back electromagnetic force (back-EMF). The proposed method maintains the minimum phase root mean square (RMS) current, and keeps the maximum efficiency under 2,500 rpm and 0 N·m to 0.8 N·m load conditions.

II. Motor Drive System Architecture

1. System Structure of PM Brushless Motor Operation

Figure 1 shows a block diagram of a PM brushless motor system. The motor system can be divided into three parts — PM brushless motor, three-phase voltage-source inverter (VSI), and sensorless sine-wave controller.

The PM brushless motor has a surface-mounted PM rotor and internal parameters such as stator resistance and inductance. The three-phase VSI is composed of six power MOSFETs with a sense-FET, which supplies power to the motor. The sensorless sine-wave controller is composed of various control blocks, such as a pulse-width modulation (PWM) generator, speed control, gate driver, open-loop start-up, position detector, and automatic lead-angle compensation. The speed control block determines the duty factor (DF) of the PWM signal by comparing the current and reference speeds. The PWM generator produces a gate control signal through the modulation of sine- and saw-waves. The gate driver gives the

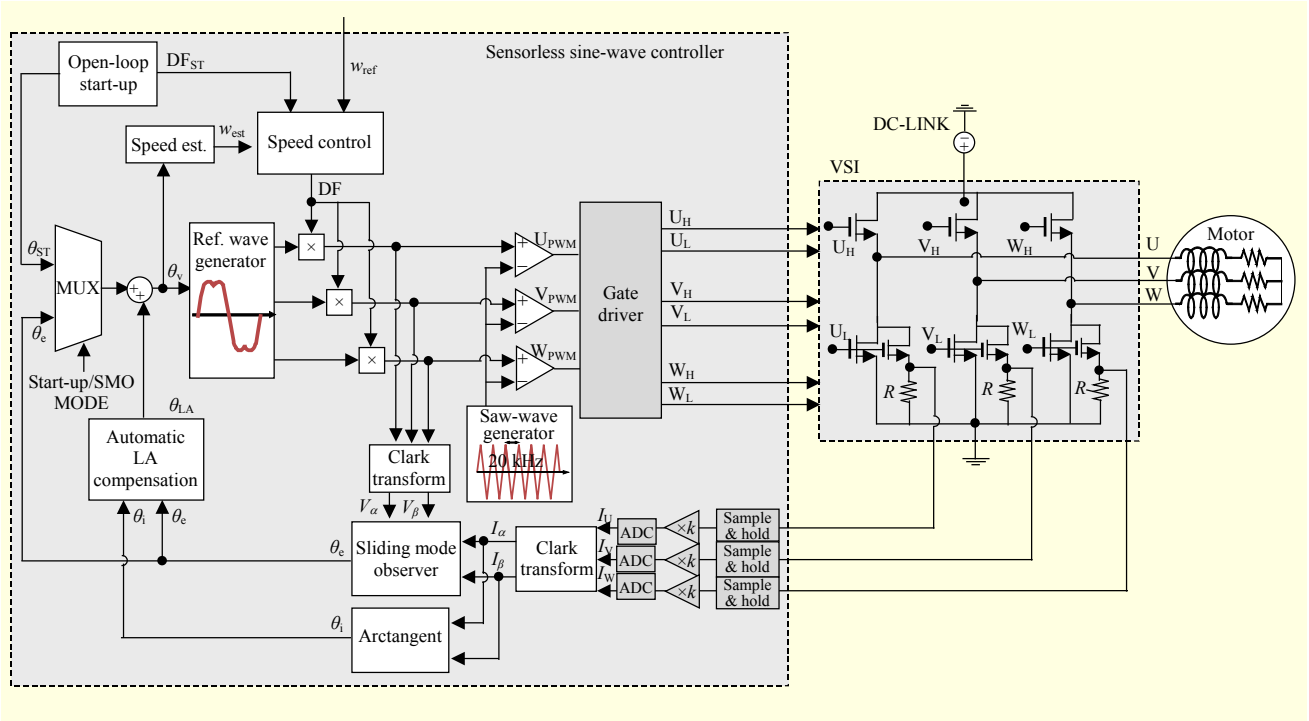

Fig. 1. Block diagram of proposed PM brushless motor system.

ETRI Journal, Volume 37, Number 6, December 2015
http://dx.doi.org/10.4218/etrij.15.0115.0329

proper driving signals from the PWM to the high/low side *n*-channel power MOSFETs in a three-phase VSI. The sensorless driving parts are designed to operate the motor without any additional sensors, such as a position or current sensor, and the position and current detections can be achieved completely using circuit techniques. An open-loop start-up algorithm assists in accelerating the motor from a standstill. To drive the motor without a position sensor, back-EMF is estimated using electrical information, such as the current and voltage. To detect the phase current, the sensing signal of the sense-FET is converted into a 10-bit current signal. A computational block, such as the Clark transform or Arctangent, helps the controller analyze the motor driving states.

2. Isolated Three-Phase Gate Driver

The three-phase gate driver is designed so as to operate a high/low side MOSFET. A circuit diagram of the U-phase gate driver is shown in Fig. 2. The gate driver receives a driving signal from the PWM generator and transforms it into a proper signal considering the states of the power devices. The gate driver of the proposed IC is designed for power devices having a gate drive of less than 5 V. A high-side gate operating signal should be generated from the floating node between the high- and low-side devices; therefore, it is necessary to use isolated devices. The isolation island of the proposed IC is considered to have a blocking voltage of approximately 100 V from the main substrate. The pulse generator makes two pulse signals at the edge of the PWM signal, which shifts the voltage level. The voltage level shifter transfers the signals to the latch and non-inverting buffer, which operate among the isolation area. The power source of the final gate signal is from the bootstrap capacitor and diode. In addition, a low-side gate operating signal is generated through a high/low delay matching circuit to avoid a conflict between signals.

3. Current Self-Sensing Method

The three-phase VSI is composed of six power devices, and each phase has high- and low-side power switches. The proposed IC is able to detect a full sine-wave current using only a low-side sensing circuit, as shown in Fig. 2, because the power switches are a bidirectional-MOSFET. Although the sense-FET shares the gate and drain with the main-FET, the size of the sense-FET is designed to be relatively smaller than that of the main-FET; therefore, the phase current is divided by the size constant (= α), whereby α is the size ratio between the main-FET and sense-FET.

When the U-phase of the low-side switch is on, the equivalent circuit of the main-FET and sense-FET is as shown in Fig. 3. Here, I_U, R_{DS}, and α are the flowing phase current, the

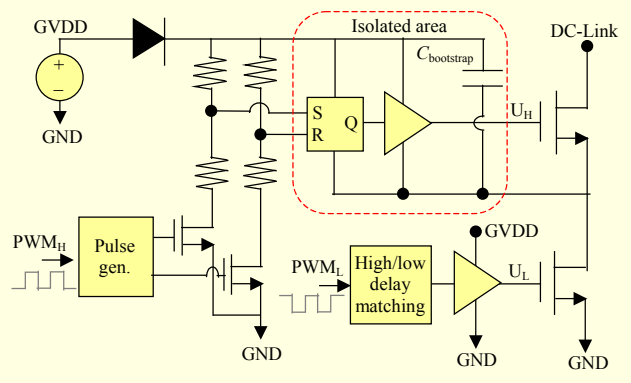

Fig. 2. Circuit diagram of U-phase gate driver.

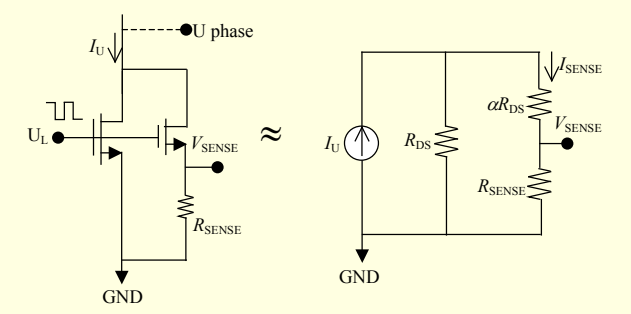

Fig. 3. Equivalent circuit of current-sensing devices when switches are on.

resistance of the main-FET, and the design ratio of the main-FET and sense-FET, respectively. The sensing voltage (V_{SENSE}), which means the current of the U-phase, is analyzed through the following equation:

$$I_{SENSE} = \frac{R_{DS} I_U}{R_{DS} + (\alpha R_{DS} + R_{SENSE})}, \tag{1}$$

$$\begin{aligned} V_{SENSE} &= \frac{R_{DS} I_U}{R_{DS} + (\alpha R_{DS} + R_{SENSE})} R_{SENSE} \\ &= \frac{R_{DS} I_U}{\frac{R_{DS}(\alpha + 1)}{R_{SENSE}} + 1}. \end{aligned} \tag{2}$$

Based on (2), V_{SENSE} is calculated based on the sensing resistance (R_{SENSE}) and can be summarized in the following three cases:

$$\begin{aligned} &\text{Case 1. } R_{SENSE} = 0 \\ &\Rightarrow V_{SENSE} = 0, \\ &\text{Case 2. } R_{SENSE} = \infty, \ (R_{SENSE} >> \alpha, R_{DS}) \\ &\Rightarrow V_{SENSE} = R_{DS} I_U, \\ &\text{Case 3. } R_{SENSE} = X R_{DS} \\ &\Rightarrow V_{SENSE} = \frac{R_{DS} I_U}{\frac{\alpha + 1}{X} + 1} = Y R_{DS} I_U, \quad \left(Y = \frac{1}{\frac{\alpha + 1}{X} + 1} \right). \end{aligned} \tag{3}$$

According to "Case 2" of (3), V_{SENSE} is approximately determined based on the relation of the on-resistance (R_{DS}) and phase current (I_U) under a high R_{SENSE} value, and is converted into data on I_U using a sample-and-hold, analog amplifier, and analog-to-digital converter.

4. Position Detecting Method

To drive the motor without a position sensor, it is necessary to estimate the back-EMF by using electrical information, such as the current and voltage. We designed the position detector by employing a sliding mode observer algorithm [16]. Figure 4 shows a block diagram of the sliding mode observer. The major three-phase variables are analyzed on an α-β stationary frame through a Clark transformation. This is the control method used to extract the position information of the rotor by tracking the error between the real (i_α, i_β) and estimated $(\hat{i}_\alpha, \hat{i}_\beta)$ currents. The sliding mode observer is suitable for a sine-wave control system because it can analyze within an α-β stationary reference frame and simple equivalent-EMF model. The analysis of the sliding mode observer has a mathematical proof, which we can describe briefly through the following equations [10], [17].

The PM brushless motor model in the stationary reference frame is

$$\begin{bmatrix} \dot{i}_\alpha \\ \dot{i}_\beta \end{bmatrix} = \frac{1}{L_s}\begin{bmatrix} v_\alpha \\ v_\beta \end{bmatrix} - \frac{R_s}{L_s}\begin{bmatrix} i_\alpha \\ i_\beta \end{bmatrix} - \frac{1}{L_s}\begin{bmatrix} e_\alpha \\ e_\beta \end{bmatrix}, \tag{4}$$

where the symbol " $\cdot$ " means the derivative of time, and i_α, i_β, v_α, v_β, e_α, e_β, R, and L are the phase current, phase voltage, and back-EMF in the stationary axis, and the motor stator resistance (Ω) and inductance (H), respectively. The current observer model in the stationary reference frame is

$$\begin{bmatrix} \dot{\hat{i}}_\alpha \\ \dot{\hat{i}}_\beta \end{bmatrix} = \frac{1}{L}\begin{bmatrix} v_\alpha \\ v_\beta \end{bmatrix} - \frac{R}{L}\begin{bmatrix} \hat{i}_\alpha \\ \hat{i}_\beta \end{bmatrix} - \frac{1}{L}\begin{bmatrix} kH(\hat{i}_\alpha - i_\alpha) \\ kH(\hat{i}_\beta - i_\beta) \end{bmatrix}, \tag{5}$$

where the symbol "^" indicates the estimated value, k is the constant gain, and H is the function of a closed loop. If the estimated value of the current is similar in value to the real current, then the back-EMF can be found through the following equations. The sliding mode surface can be defined as

$$s_n = [s_\alpha \ s_\beta]^{\mathrm{T}}, \tag{6}$$

where $s_\alpha = i_\alpha - \hat{i_\alpha}$ and $s_\beta = i_\beta - \hat{i_\beta}$. A Lyapunov function can help in finding the existence of the sliding mode.

$$V = \frac{1}{2}s_n^{\mathrm{T}}s_n = \frac{1}{2}\left(s_\alpha^2 + s_\beta^2\right). \tag{7}$$

From the Lypunov stability theorem [10], [17], the sliding-mode condition can be induced to satisfy the condition in which $\dot{V} < 0$ for $V > 0$. As a result, the sliding mode occurs under the conditions $k \geq (|e_\alpha|, |e_\beta|)$, and we can find the back-EMF signal as

$$kH\left(\hat{i}_\alpha - i_\alpha\right) \cong e_\alpha, \tag{8}$$

$$kH\left(\hat{i}_\beta - i_\beta\right) \cong e_\beta. \tag{9}$$

In addition, we can deduce the rotor position more exactly using the arctangent function,

$$\theta_e = \tan^{-1}(e_\beta / e_\alpha). \tag{10}$$

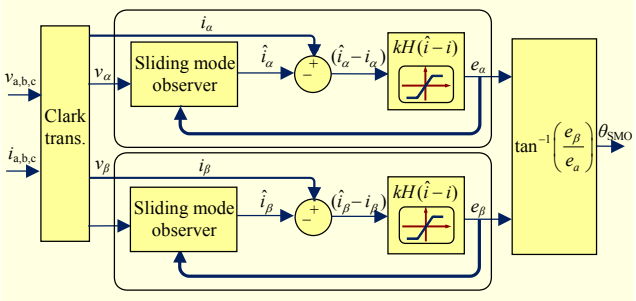

Fig. 4. Block diagram of sliding mode observer.

5. Open-Loop Start-Up Method

For the sensorless driving of the PM brushless motor, the start-up algorithm assists in detecting the condition of the back-EMF signal. Because the back-EMF can take place under a varying magnetic flux, the magnetic rotor should be rotated using a start-up sequence before obtaining the back-EMF signal. The proposed driver includes a V/f-based open-loop start-up, which forces the three-phase voltage signal to be applied according to the operating frequency. The open-loop start-up has a three-step sequence. To proceed with the start-up sequence, variables such as the position/DF are calculated at each step. Figure 5 shows the driving statement during start-up sequence.

Figure 5 shows the driving statement during start-up sequence. The unpredictable position at a standstill motor aligns to that of a designated position during the first step (step 1). This step maintains a constant value for the DF and zero acceleration and speed.

$$\theta_{ST} = \theta_{initial}\,(\mathrm{rad}), \tag{11}$$

$$\mathrm{DF} = \mathrm{DF}_{minimum}\,(\%), \tag{12}$$

where $\theta_{initial}$ and $\mathrm{DF}_{minimum}$ are the initial position for alignment and the minimum value of the DF, respectively.

In the second step (step 2), the motor is accelerated to a reference speed from a standstill using the calculated open-loop

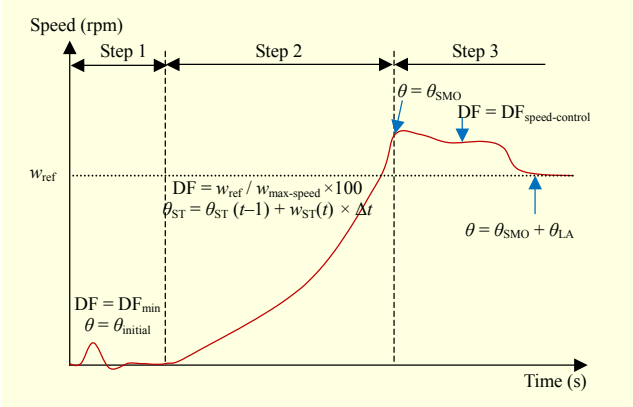

Fig. 5. Driving statement during start-up sequence.

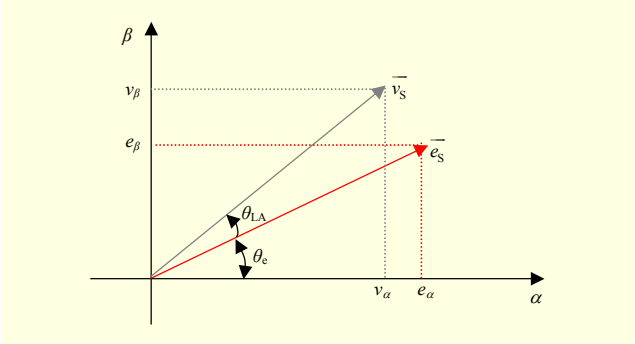

Fig. 6. Lead-angle of PM brushless motor on stationary reference coordinate.

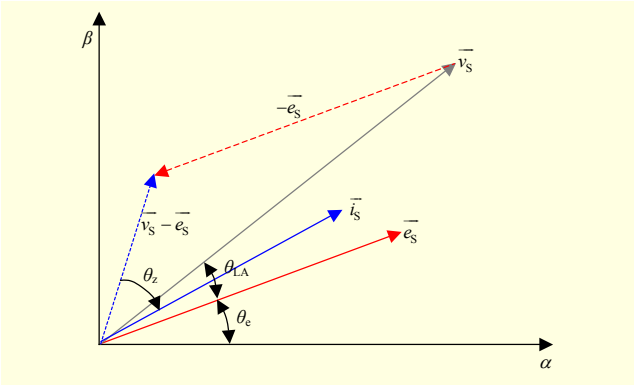

Fig. 7. Current state diagram in stationary reference coordinate.

position signal and DF. The driving algorithm in step 2 is based on the following equations:

$$a_{\text{start-up}} = \frac{\omega_{\text{ref}}}{\Delta t_{\text{step-2}}} \,(\text{rad}/\text{s}^2), \tag{13}$$

$$\omega_{\text{ST}}(n) = \omega_{\text{ST}}(n-1) + a_{\text{start-up}} \times \Delta t_{\text{clk}}\,(\text{rad}/\text{s}), \tag{14}$$

$$\theta_{\text{ST}}(n) = \theta_{\text{ST}}(n-1) + \omega_{\text{ST}}(n) \times \Delta t_{\text{clk}}\,(\text{rad}), \tag{15}$$

$$\text{DF} = \frac{100}{\omega_{\text{max-speed}}} \times \omega_{\text{ref}}\,(\%), \tag{16}$$

where n is the calculated sequence based on the clock, and $a_{\text{start-up}}$, ω_{ref}, ω_n, θ_n, Δt_{clk}, and $\Delta t_{\text{step-2}}$ are the acceleration, reference speed, speed of n, position of n, time duration of the calculating clock, and time duration of step 2, respectively. The DF is calculated based on the constant V/f ratio, which controls the voltage amplitude using a sinusoidal PWM modulator based on the frequency of the motor speed.

In the third step (step 3), the open-loop position signal is changed to a real position signal from the sliding mode observer and speed control, and the automatic lead-angle algorithm starts to operate.

III. Automatic Lead-Angle Compensation

1. Lead-Angle Definition

The lead-angle (θ_{LA}) can be defined as the value of the advanced angle relative to the rotor position. In a sensorless driving state, the motor is controlled by the phase of the back-EMF (θ_{e}) as the rotor position signal. Figure 6 shows the meaning of the lead-angle by displaying the relationships of the applied voltage and back-EFM waves on the α-β stationary reference coordinate, where e_{s}, v_{s}, θ_{e}, and θ_{LA} are the vectors of the back-EMF and applied voltage, and phases of the back-EMF and lead-angle, respectively.

The phase of the applied voltage (θ_{v}) is changed by the lead-angle (θ_{LA}), which can be expressed as

$$\theta_{\text{v}} = \theta_{\text{e}} + \theta_{\text{LA}}. \tag{17}$$

The lead-angle (θ_{LA}) affects the motor driving conditions because a variation in lead-angle (θ_{LA}) changes the state of the voltage (v_{s}), which influences the state of the current (i_{s}) through the relationships with the back-EMF (e_{s}) and impedance (z_{s}), as in the following equation:

$$\vec{i}_{\text{s}} = \left(\vec{v}_{\text{s}} - \vec{e}_{\text{s}}\right) / \vec{z}_{\text{s}}, \tag{18}$$

where $\vec{z}_{\text{s}}$ is the stator impedance with resistance (R_{S}) and inductance (L_{S}) of the motor, which can be defined as the amplitude ($|z_{\text{s}}|$) and phase (θ_{z}) based on phasor diagrams and electrical theory. From the complex domain of the phase theory, the real value of the impedance is matched on the α-axis, and the imaginary value of the impedance is matched on the reverse β-axis. To be specific, the phase of current (θ_{i}) is calculated based on the relationship between the vector difference of the voltage (v_{s}) and back-EMF (e_{s}) and the phase of the impedance (θ_{z}), as shown in Figure 7.

If the operating velocity and applied load are stable, then the

applied voltage (v_s) is the only control variable in the VSI. Concretely, for the amplitude ($|v_s|$) and phase (θ_v) of the applied voltage, both parameters determine the state of the phase current (i_s). The applied voltage can be generated through the VSI by the PWM signal, and the effective amplitude ($|v_s|$) is defined by the PWM DF. The phase of the applied voltage (θ_v) is controllable based on the rotor position estimation (θ_e) and lead-angle (θ_{LA}), as illustrated in (17).

2. High Efficiency Operating Method

The efficiency of the motor driving can be calculated by the output power and loss. Generally, motor losses are divided into copper loss and iron loss. The iron loss is based on motor structure and fabrication as follows:

$$P_{\text{iron-loss}} = K_e f^2 B_m^2 + K_h f B_m^2 ,$$

where, K_e is the eddy-current loss coefficient, K_h is the hysteresis loss coefficient, f is switching frequency, and B_m is the maximum magnetic flux density. The variables K_e and K_h are decided by the loss curve of the magnetic core in a motor.

The copper loss is defined as follows:

$$P_{\text{copper-loss}} = 3 I_{\text{rms}}^2 R , \quad (19)$$

where I_{rms} is the RMS value of the phase current and R is the stator resistance. Because the copper loss can be increased according to the high current driving, it is necessary to reduce the phase current during motor driving.

To analyze the mechanical output of the motor, the torque can be expressed as

$$T_e = \left(e_a i_a + e_b i_b + e_c i_c \right) / w_e , \quad (20)$$

where T_e is electric torque, $e_{a,b,c}$ is the back-EMF, and w_e is angular velocity. The amount of torque induced is directly calculated by the correlation of the back-EMF and phase current, as in (20). To reach a reference speed during the acceleration period, a torque higher than the shaft load should be induced, and after a steady-state period, the torque should be made similar to the shaft load. When copper loss is considered, an efficient motor control is used to induce a large torque through a small current. From (20) above, the phase of the back-EMF (θ_e) and the phase current (θ_i) should be matched equally to induce the optimal torque for the most efficient drive. Therefore, the phase difference of the back-EMF (θ_e) and phase current (θ_i) have to be controlled to zero by adjusting the lead-angle (θ_{LA}) of the applied voltage.

3. Automatic Lead-Angle Compensation Algorithm

We proposed and designed a method of automatic lead-angle compensation for high-efficiency motor driving under a wide range of torque-speed conditions. The automatic lead-angle compensation controls the phase of applied voltage so that the phase of the current is intentionally adjusted.

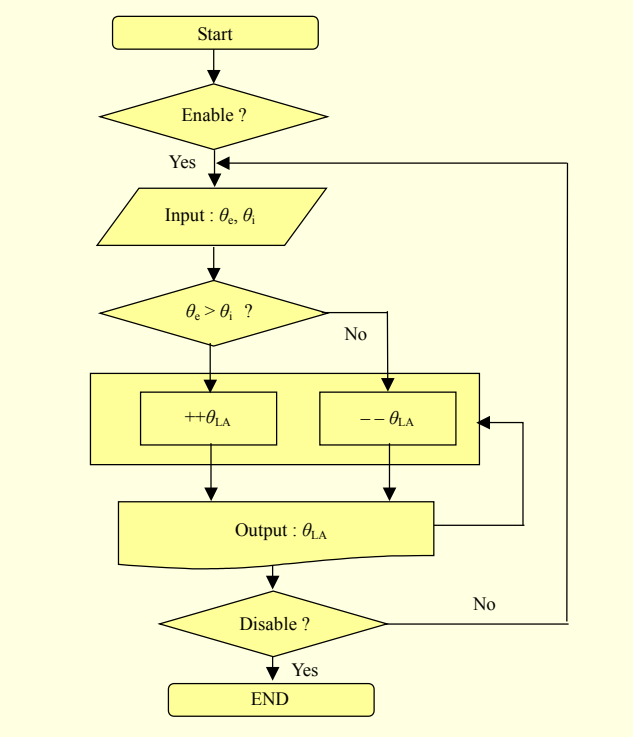

Fig. 8. Algorithm flowchart of automatic lead-angle method.

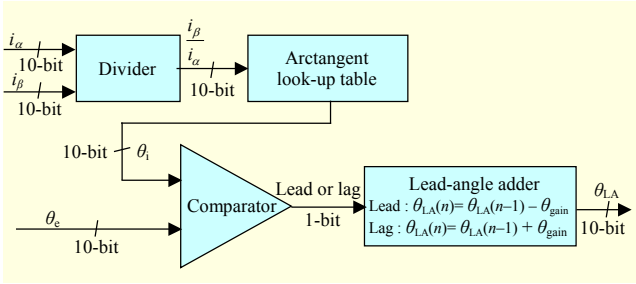

Fig. 9. Digital circuit diagram of automatic lead-angle compensator.

To achieve efficient torque-speed characteristics, the phase of the phase voltage (θ_v) should be automatically shifted by controlling the lead angle, which reduces the phase difference between the back-EMF and phase current. Figure 8 shows a flow chart of the automatic lead-angle compensation algorithm. Using the algorithm of Fig. 8, the lead angle is continuously calculated by comparing the phase difference between the back-EMF and current.

The automatic lead-angle compensator was designed with digital circuits using the block diagram shown in Fig. 9. To calculate the phase of the current, an arctangent block composed of a divider and look-up table was designed. The phase of the back-EMF is the output of the sliding mode

ETRI Journal, Volume 37, Number 6, December 2015
http://dx.doi.org/10.4218/etrij.15.0115.0329

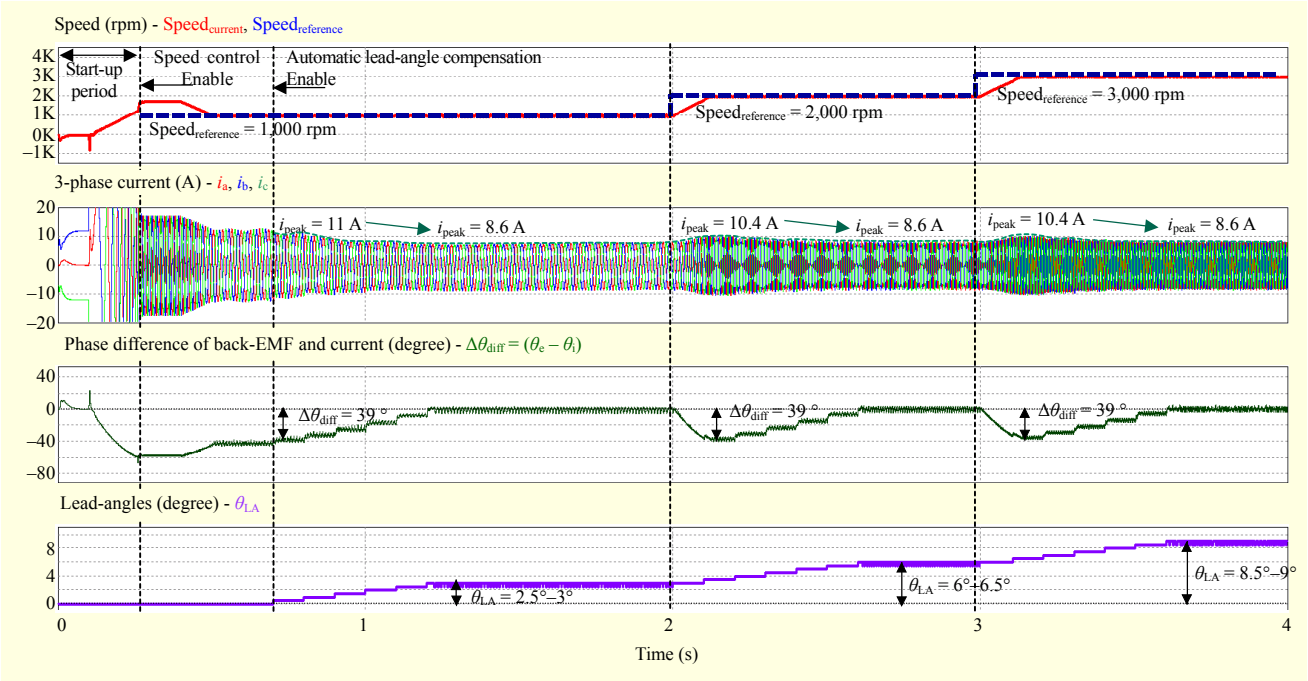

Fig. 10. Simulation results of proposed motor driving system.

observer, and the lead-lag statement between the back-EMF and current is distinguished by the comparator. The output data of the lead-angle are calculated by adding/subtracting the constant values, which can be used to track the optimum condition of the motor driving environment.

IV. Simulation Results

Sensorless sine-wave control of a PM brushless motor system was verified through a PSIM simulator, version 9.0. The simulation conditions of the motor system were established, as shown in Table 1, and are similar to the real motor used in the experiment. The PSIM library conveniently provided the PMSM motor, power MOSFET, and gate driver. The motor control algorithms, including the automatic lead-angle compensator, start-up, and sliding mode observer, were designed using a C-language-based implementation.

Figure 10 shows the simulation results of the motor system operation from start-up to the reaching of a reference speed, including the results of the motor speed; current; phase difference of the back-EMF and current; and lead-angle when the motor speed increased from 1,000 rpm to 3,000 rpm. An automatic lead-angle compensator was successfully achieved by reducing the phase difference of the back-EMF (θ_e) and the phase current (θ_i) under the given speed control conditions.

The conventional method with fixed lead-angles and the proposed method with automatic lead-angle compensation were compared through PSIM simulations. Figure 11 shows the amplitude of the phase current according to the lead-angle values under various motor speed/load conditions. The automatic lead-angle compensator changes the lead-angle automatically depending on the motor speed, and each value is coincident to the optimum point of the conventional fixed lead-angle values under 100 mN·m, 300 mN·m, 500 mN·m and 1,000 rpm, 2,000 rpm, 3,000 rpm conditions, as shown Fig. 11.

Table 1. Simulation conditions of motor control system.

Conditions	Values
Rated power	SPMSM 200 W
Poles	4 poles
Resistance	0.09 Ω
Inductance	270 μH
Back-EMF constant	4.58 V_{PP}/krpm
Demonstration tool	PSIM 9.0

V. Experimental Results

1. Fabrication of Motor Controller

To evaluate the proposed motor driving algorithm, sensorless sine-wave controller ICs were fabricated through a DBH 0.18 μm BCDMOS process. As shown in Fig. 12, the ICs occupy a die area of 4.3 mm × 3.0 mm and consist of

digital/analog mixed circuits. The digital part of a fabricated IC includes an automatic lead-angle compensator, sliding mode observer, speed controller, PWM modulator, and start-up algorithm. They were designed as having 51,351 gates using

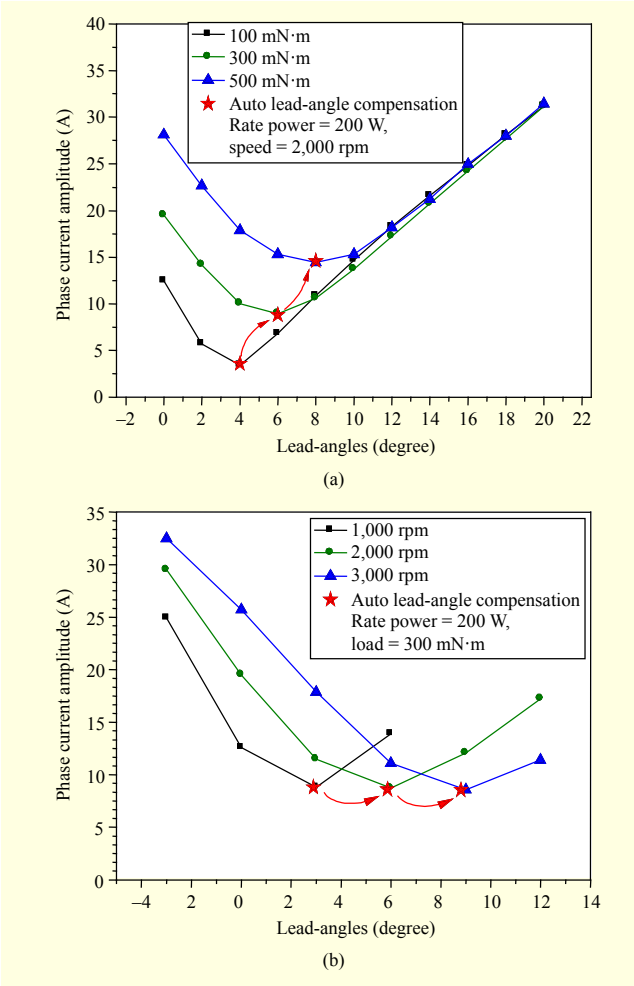

Fig. 11. Amplitude of phase current according to lead-angle under (a) various speed and (b) load conditions.

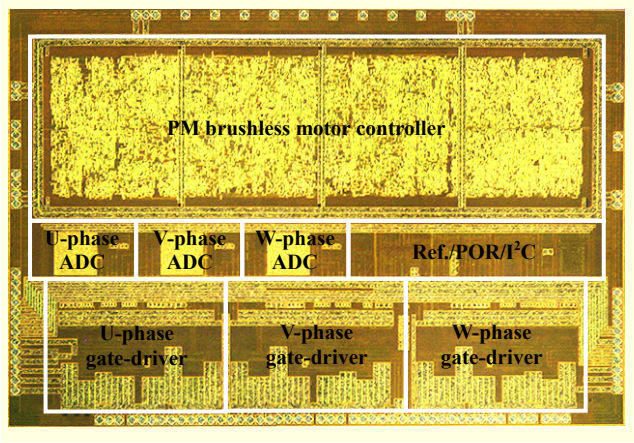

Fig. 12. Die microphotograph of fabricated motor control IC.

Table 2. Experimental conditions of motor control system.

Conditions	Values
Motor rate power	200 W
Motor poles	4 poles
Motor resistance	0.09 Ω
Motor inductance	270 μH
Back-EMF constant	4.58 V_{PP}/krpm
DC-Link	24 V
Power devices	100 V MOSFET NXP Semiconductor
Motor controller	Proposed IC (ETRI MA1608)

the DBH 1.8 V standard library. The analog part of a fabricated IC includes a gate driver, amplifiers for the current sensing, and a 10-bit SAR type analog-to-digital converter, which were designed based on the DBH 1.8/5 V standard library. The ICs are operated at 20 MHz and the operating commands are delivered using an I^2C serial interface from a personal computer.

2. Motor Controller Test and Performance

To verify the fabricated motor control IC, the experimental environment was built as shown in Table 2 and Fig. 13. The sensorless sine-wave controller was completely operated under 200 W of rated power and speed control conditions. The VSI consists of a commercial 100 V power MOSFET with a sense-FET. The mechanical motor consists of a commercial 200 W permanent magnetic brushless motor with electrical loads. A motor system efficiency measurement, which is the so-called NTI test, was conducted using the dynamometer at the Korea Electronics Technology Institute in the Republic of Korea.

To investigate the effect of an automatic lead-angle compensator, the system efficiency and phase current were measured under a wide range of load conditions.

Conventional control methods with six to ten degrees of fixed lead-angles and automatic lead-angle compensation were measured using the dynamometer at under 2,500 rpm and

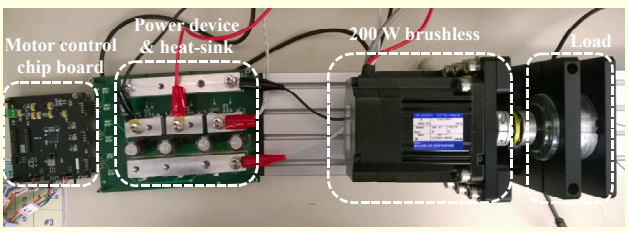

Fig. 13. Experimental configuration of motor driving system.

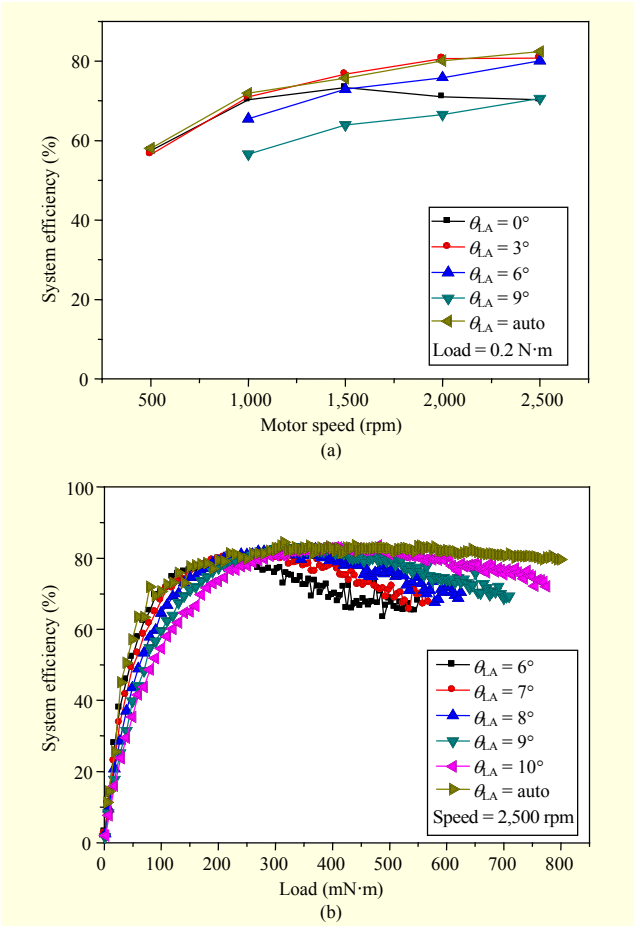

Fig. 14. System efficiency of lead-angle (θ_{LA}) condition under (a) 2,500 rpm and (b) 0 N·m to 0.8 N·m load.

0 N·m to 0.8 N·m load conditions. The dynamometer measured the electrical and mechanical characteristics, and therefore the efficiency of the motor system was obtained as follows.

The system efficiency can be defined through the following equations:

$$P_{DC} = V_{DC} \times I_{DC} \ (\mathrm{W}), \tag{21}$$

$$P_{MOTOR} = T_m \times w_m \ (\mathrm{W}), \tag{22}$$

$$\eta_{system} = P_{MOTOR} / P_{DC} \ (\%), \tag{23}$$

where P_{DC} is the electrical input power, P_{MOTOR} is the motor output power, η_{system} is the system efficiency, V_{DC} is the DC-Link voltage, I_{DC} is the input average current, T_m is the motor torque, and w_m is the motor speed.

Figure 14 shows the motor efficiency found in the experimental results. The automatic lead-angle method closely tracked the maximum value of various fixed lead-angle conditions. The proposed system maintained an 80% motor

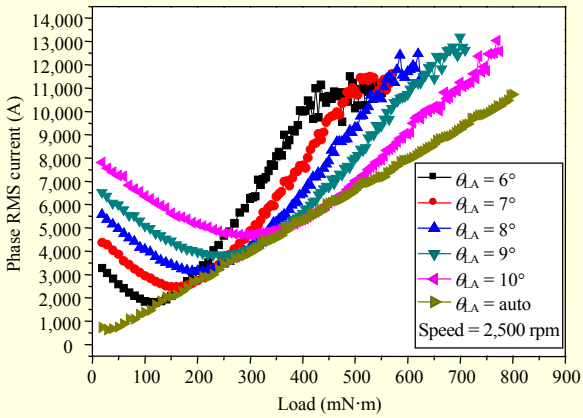

Fig. 15. Phase RMS current of lead-angle (θ_{LA}) conditions under 2,500 rpm and 0 N·m to 0.8 N·m load.

efficiency under load conditions of 0.2 N·m to 0.8 N·m and speed conditions of 500 rpm to 2,500 rpm.

The phase RMS currents of the experiment drives were measured as shown in Figure 15. The automatic lead-angle method maintained the minimum phase RMS current, while the conventional methods had a relatively high current under both low and high load conditions. This means that the copper loss can be minimally maintained using an automatic lead-angle compensation, as shown in (19).

VI. Conclusion

We proposed and demonstrated a sensorless sine-wave controller for a PM brushless motor employing an automatic lead-angle compensator. For driving the sensorless sine-wave motor, we proposed a controller IC including an open-loop start-up and position detector with a sliding mode observer. The proposed controller was applied to a 200 W PM brushless motor system and was demonstrated through motor dynamo measurements. The automatic lead-angle compensation method maintained the minimum phase RMS current and 80% motor efficiency under load conditions of 0 N·m to 0.8 N·m. The proposed PM brushless motor driving method is suitable for manufacturing a motor control SoC for various applications within a wide range of load and speed conditions.

References

[1] R. Saidur, "A Review on Electrical Motors Energy Use and Energy Savings," *Renewable Sustain. Energy Rev.*, vol. 14, no. 3, Apr. 2010, pp. 877–898.

[2] F. Magnussen and C. Sadarangani, "Winding Factors and Joule Losses of Permanent Magnet Machines with Concentrated Windings," *IEEE Int. Electr. Mach. Drives Conf.*, Madison, WI,

USA, June 1–4, 2003, pp. 333–339.

[3] T.M. Jahns, G.B. Kliman, and T.W. Neumann, "Interior Permanent Magnet Synchronous Motors for Adjustable-Speed Drives," *IEEE Trans. Ind. Appl.*, vol. 1A-22, no. 4, July–Aug. 1986, pp. 738–747.

[4] L. Parsa and H.A. Toliyat, "Five-Phase Permanent-Magnet Motor Drives," *IEEE Trans. Ind. Appl.*, vol. 41, no. 1, Jan.–Feb. 2005, pp. 30–37.

[5] K.I. Na et al., "Electrical Characteristics of Triple-Gate RSO Power MOSFET (TGRMOS) with Various Gate Configurations and Bias Conditions," *ETRI J.*, vol. 35, no. 3, June 2013, pp. 425–430.

[6] R.R. Tummala et al., "The SOP for Miniaturized, Mixed-Signal Computing, Communication, and Consumer Systems of the Next Decade," *IEEE Trans. Adv. Packa*g., vol. 27, no. 2, May 2004, pp. 250–267.

[7] K.-Y. Cheng and Y.-Y Tzou, "Design of a Sensorless Commutation IC for BLDC Motors," *IEEE Trans. Power Electron.*, vol. 18, no. 6, Nov. 2003, pp. 1365–1375.

[8] S.-L. Chen, C.K. Lee, and H.-H Chen, "Implementation of a Single-Chip Design for the Three-Phase Brushless-DC-Motor (BLDC) System," *SoC Des. Conf. ISOCC*, Busan, Rep. of Korea, Nov. 17–19, 2013, pp. 108–112.

[9] B.-H. Bae et al., "Implementation of Sensorless Vector Control for Super-High-Speed PMSM of Turbo-Compressor," *IEEE Trans. Ind. Appl.*, vol. 39, May 2003, pp. 811–818.

[10] H. Kim, J. Son, and J. Lee, "A High-Speed Sliding-Mode Observer for the Sensorless Speed Control of a PMSM," *IEEE Trans. Ind. Electron.*, vol. 58, no. 9, Sept. 2011, pp. 4069–4077.

[11] S. Morimoto et al., "Sensorless Control Strategy for Salient-Pole PMSM Based on Extended EMF in Rotating Reference Frame," *IEEE Trans. Ind. Appl.*, vol. 38, no. 4, July–Aug. 2002, pp. 1054–1061.

[12] P.D.C. Perera et al., "A Sensorless, Stable V/F Control Method for Permanent-Magnet Synchronous Motor Drives," *IEEE Trans. Ind. Appl.*, vol. 39, no. 3, May–June 2003, pp. 783–791.

[13] S.-C. Agarlita et al., "Stale V/F Control System with Controlled Power Factor Angle for Permanent Magnet Synchronous Motor Drives," *IET Electr. Power Appl.*, vol. 7, no. 4, Apr. 2013, pp. 278–286.

[14] T. Yamane, S. Ikeda, and A. Nakagawa, "Three-Phase Sinusoidal Current PWM Brushless Motor Driver ICs," in *Proc. of Int. Symp. Power Semicond. Devices ICs*, Kitakyushu, Japan, May 24–27, 2004, pp. 147–150.

[15] K. Nagai et al., *Motor Contr. Device*, US Patent 11/372,216, filed Mar. 10, 2006, issued Dec. 28, 2006.

[16] M.P. Kazmierkowski and L. Malesani, "Current Control Techniques for Three-Phase Voltage-Source PWM Converter: A Survey," *IEEE Trans. Ind. Electron.*, vol. 45, no. 5, Oct. 1998, pp. 691–703.

[17] G. Foo and M.F. Rahman, "Sensorless Sliding-Mode MTPA Control of an IPM Synchronous Motor Drive Using a Sliding-Mode Observer and HF Signal Injection," *IEEE Trans. Ind. Electron.*, vol. 57, no. 4, Apr. 2010, pp. 1270–1278.

[18] A. Tozune and T. Takeuchi, "Improvement of Torque-Speed Characteristics of Brushless Motor by Automatic Lead Angle Adjustment," *Int. Power Electron. Motion Contr. Conf.*, Xi'an, China, Aug. 14–16, 2004, pp. 583–587.

[19] C.-L Chiu et al., "An Accurate Automatic Phase Advance Adjustment of Brushless DC Motor," *IEEE Trans. Magn.*, vol. 45, no. 1, Jan. 2009, pp. 120–126.

Minki Kim received his BS degree in electrical engineering and computer science from Kyungpook National University, Daegu, Rep. of Korea, in 2008 and his MS degree in electrical engineering and computer science from Seoul National University, Rep. of Korea, in 2010. Since 2010, he has been working at ETRI as a researcher. His research interests include wide band-gap power devices and power control systems.

Sewan Heo received his BS and MS degrees in electrical and electronic engineering from the Korea Advanced Institute of Science and Technology, Daejeon, Rep. of Korea, in 2005 and 2007, respectively. He joined ETRI in 2007, where he is currently a senior researcher. His research interests include power converters, synchronous motor drives, digital/analog control circuits design, and renewable energy conversion in power systems.

Jimin Oh received his BS degree in electrical and electronic engineering and his MS degree in electrical engineering from Kyoto University, Japan, in 2008 and 2010, respectively. Upon graduating, he joined ETRI as a researcher. His research interests include motor driver IC design, power management IC design, nonlinear dynamics, and MEMS.

Jung-Hee Suk received his BS, MS, and PhD degrees in electronics engineering from Kyungpook National University, Daegu, Rep. of Korea, in 2001, 2003, and 2007, respectively. His doctoral research involved the H.264/AVC codec algorithm. He joined ETRI in February 2007 as a researcher and now works for the NT Convergence Components Research Department. His current research interests include multimedia codecs; parallel processing of media data; efficient architectures of SoC; recognition algorithms for smart vehicles and mobile terminals; and motor control systems.

Yil Suk Yang received his BS, MS, and PhD degrees in electronics engineering from Kyungpook National University, Daegu, Rep. of Korea, in 1989, 1994, and 2008, respectively. Before joining ETRI in 1999, he was with LG Semiconductor, Seoul, Rep. of Korea. Since 1999, he has worked at ETRI's Basic Research Laboratory, where he has been engaged in research on low power circuit design, high energy efficiency circuit design, and power electronics design.

Ki-Tae Park received his BS degree and MS degrees at the Department of Electrical Engineering from Seoul National University, Rep. of Korea, in 1995 and 1997, respectively. Since 1997, he had worked for Samsung Electronics, Co., Ltd., Suwon, Rep. of Korea until he founded Iron Device Corporation, Seoul, Rep. of Korea in 2008, where he is CEO. His interests include mixed signal system LSI design, audio power amplifier IC, and power electronics.

Jinsung Kim received his BS degree at the Department of Electrical Engineering from Konkuk University, Seoul, Rep. of Korea, in 1998. From 1998 to 1999, he had worked for Samsung Electronics, Co., Ltd., Suwon, Rep. of Korea. From 2009 to 2008, he had worked for Fairchild Korea, Co., Ltd., Bucheon, Rep. of Korea. Since 2008 he has worked at Iron Device Corp., Seoul, Rep. of Korea as a circuit designer. His interests include mixed signal system LSI design, class D audio amplifier, and power electronics.